Supporting Information

Dynamic Surface Reconstruction Engineers Interfacial Water Structure for Efficient Alkaline Hydrogen Oxidation

Chaoyi Yang, Zihao Dai, Jianchao Yue, Guangqin Wang and Wei Luo*

Experimental Procedures

Reagents and materials

Platinum bis(acetylacetonate) [$Pt(acac)_3$, ~98%, Wuhan, Changcheng Chemical Co., Ltd.], Selenium [Se, ~99%, China, Sinopharm Chemical Reagent Co., Ltd], Oleylamine [OAm, 80%~90%, Aladdin Industrial Co. Ltd], ethanol, n-hexane and isopropanol [>99% and ~99.5%, China, Sinopharm Chemical Reagent Co., Ltd.], Support: carbon black (Vulcan, XC-72R). The water used in all experiments was prepared by passing through an ultra-pure purification system.

Synthesis of $PtSe_x$ (x=1.5, 2, 3)

Typically, OAm (5.0 ml), $Pt(acac)_2$ (19.7 mg), XC-72 carbon (39 mg) and different ratio of Se (5.6 mg, 8.4 mg and 11.2 mg corresponding to $PtSe_{1.5}$, $PtSe_2$ and $PtSe_3$) were added to the three-neck flask and stirred magnetically. The mixture was heated to 100 °C and maintained in this temperature for 30 minutes under vacuums conditions to remove the moisture and oxygen in the reaction system. The mixture was heated to 260 °C and maintained for 1h under the protection of N_2. After cooling down naturally, the obtained black product was collected by centrifugation with adding n-hexane and ethanol for five times and then dried at room temperature under vacuum. Finally, the dried products were annealed under the gas atmosphere (5% H_2, 95% N_2) at 350 °C for 30 min to obtain the $PtSe_x$.

Physical characterizations

The Powder X-ray diffraction (XRD) patterns were collected by an obtained on a Bruker D8-Advance X-ray diffractometer with a Cu Kα radiation source (λ = 0.154178 nm). The transmission electron microscopy (TEM) images were performed with JEM-2100 Plus operated at 200 kV. Scanning transmission electron microscopy (STEM)

imaging and energy-dispersive X-ray spectroscopy (EDX) mapping were acquired on a JEOL JEM-ARM200CF microscope operated at 200kV with a Schottky cold-field emission gun. X-ray photoelectron spectroscopy experiments were collected with Thermo Fisher ESCALAB 250Xi using Al Kα radiation source. Inductively coupled plasma atomic emission spectroscopy (ICP-AES) were conducted on a Thermo IRIS Intrepid II XSP atomic emission spectrometer. X-ray absorption spectroscopy (XAS) including both X-ray absorption near-edge structure (XANES) and extended X-ray absorption fine structure (EXAFS) at Pt L-edge were collected in total-fluorescence-yield mode at ambient air at the BL11B beamline of the Shanghai Synchrotron Radiation Facility (SSRF). In situ surface-enhanced infrared absorption spectroscopy (SEIRAS) was carried out with Bruker Invenio R equipped with a liquid nitrogen-cooled detector. A homemade IR cell with a polished Si prism was employed as experimental apparatus.

Electrochemical measurements

All the electrochemical measurements were conducted by the CHI 760E electrochemical analyzer (CH Instruments, Chenhua Co., Shanghai, China). The standard three-electrode-system were adopted. Glass carbon electrode (GCE, diameter: 5 mm) with catalysts coating were used as the working electrode. The Hg/HgO electrode (MOE) (in 0.1 M KOH or 1.0 M KOH) and the graphite rod were served as reference electrode in alkaline electrolytes and the counter electrode, respectively. All measured potentials were reported versus the reversible hydrogen electrode (RHE) potential.

To prepare catalyst ink for HOR experiments, 4 mg catalysts were dispersing in 2 ml isopropanol solution containing 0.05% Nafion. The mixture solvent was ultrasonicated for 1h to form homogeneous solution. Then, 5 μL ink was pipetted onto the surface of glassy carbon electrode (GCE, 5 mm in diameter) resulting in a total mass loading of ~ 0.05 mg cm^{-2}_{geo}. The accurate loading of catalysts and elements contents were originated from the ICP-AES results listing in Table S1.

Cyclic voltammetry (CV) was conducted in 0.1 M KOH solution with Ar-saturated at

a scanning rate of 50 mV s^{-1} from 0 V to 1.2 V. The HOR polarization curves were recorded by a rotation disk electrode (RDE) with a rotation speed of 1600 rpm in a H_2-saturated 0.1 M KOH and the potential range is from -0.08 V to 1.2 V at a scanning rate of 10 mV s^{-1}.

Exchange current density (j^0) obtained from linear fitting of micropolarization regions (−5 to 5 mV), through the simplified Bulter–Volmer equation (Eq. S1) [1]:

$$j = j^0 \frac{\eta F}{RT} \qquad \text{.....Eq. S1}$$

Where R equals the universal gas constant, T equals the temperature in the Kelvin scale, F equals Faraday's constant, j equals the measured current density, and η equals the applied overpotential.

The HOR polarization under the rotation speed of 2500, 2025, 1600, 1225, 900, 625 and 400 rpm were collected at a scanning rate of 10 mV s^{-1}. The kinetic current density (j^k) of each electrocatalyst could be calculated from the Koutecky-Levich equation (Eq. S1) [2]

$$\frac{1}{j} = \frac{1}{j^k} + \frac{1}{j^d} = \frac{1}{j^k} + \frac{1}{Bc_0\omega^{1/2}} \qquad \text{……Eq. S2}$$

where j and j^d are the measured and diffusion limited current density, and B represents the Levich constant, c_0 represents the solubility of H_2 (7.33×10^{-4} mol L^{-1}), ω is the rotating speed. Among them, B could be obtained from Eq. S2

$$B = 0.2nFD^{2/3}v^{-1/6} \qquad \text{…… Eq. S3}$$

where n is the numbers of electron transferred, F is the Faraday constant (96485 C mol^{-1}), D is the diffusivity of H_2 (3.7×10^{-5} cm^2 s^{-1}), and v represents the kinematic viscosity (1.01×10^{-2} cm^2 s^{-1}). [3]

Exchange current density (j^0) could be deduced from the Butler–Volmer equation in Eq. S3,

$$j^k = j^0[e^{\frac{\alpha F}{RT}\eta} - e^{\frac{-(1-\alpha)F}{RT}\eta}] \qquad \text{……Eq. S4}$$

where α is the transfer coefficient, R represents the universal gas constant (8.314 J mol^{-1} K^{-1}), T stands the operating temperature (303.15 K), η is the overpotential. [4]

Correspondingly, the Cu-UPD method is employed to determine the ECSA for the catalysts. [5] The catalysts modified electrode were cycled between 0.30 and 1.2 V in Ar-saturated solution of 0.1 M H_2SO_4 with 2 mM $CuSO_4$ to obtain a complete CV containing the UPD and overpotential deposition (OPD) of Cu. Since the stripping peaks of Cu-UPD and Cu-OPD are recorded separately, after eliminated the effect of Cu-OPD in the manner of performing the CV from 0.2 V, the region of Cu-UPD is used to calculate the ECSA. Before the deposition fo Cu, the modified electrodes were cycled between 0 and 1.2 V in pure 0.1 M H_2SO_4 as the background. The surface charge density of 420 μC cm^{-2} is assigned as a monolayer adsorption of Cu on catalysts. The value of ECSAs could be calculated via Eq. S5:

$$ECSA\left(\frac{cm^2_{metal}}{g_{metal}}\right) = \frac{Q_{Cu}}{M_{metal}\,420C\,cm^{-2}} \qquad \text{.....Eq. S5}$$

where M_{metal} is the mass loading of metals on the electrode.

For the CO stripping experiments, the samples were kept at 0.1 V versus RHE for 10 min in the saturated CO to adsorb CO on the metal surface, [6] followed by pumping Ar for 20 min to remove residual CO in the electrolyte. The CO stripping current was collected through cyclic voltammetry in a potential range from 0 to 1.2 V at a scanning rate of 5 mV s^{-1}.

The stability of catalyst was appraised by the accelerated durability tests by scanning the potential between 0 and 1.2 V for 1000 cycles at the scanning rate of 100 mV s^{-1}. Then, the HOR polarization curve was recorded in H_2-saturated 0.1 M KOH electrolyte at 10 mV s^{-1} from -0.08 to 1.2 V via the comparison with the initial curve. The loading of catalyst is around 30 μg cm_{disc}^{-2}.

In this work, all the potentials in HOR tests were referred to reversible hydrogen electrode (RHE) with *i*R-compensation. The uncompensated resistance (R_u) was measured by the electrochemical impedance spectra (EIS) tests. EIS tests were measured from 200 kHz to 0.1 kHz at a voltage perturbation of 5 mV after each RDE measurement. The *iR*-free potential ($E_{iR\text{-}free}$) was obtained by using the value of the real part of the resistance at 1 kHz, according to the following equation, Eq. S6,

$$E_{iR-free} = E - iR_u \qquad \text{Eq. S6}$$

where E, i are the measured potential and the corresponding current.

Computational methods

Density functional theory (DFT) with the Perdew-Burke-Ernzerhof (PBE) and generalized gradient corrected approximation (GGA) was carried out for electronic structure calculations. [7-8] The cutoff energy was 400 eV and the self-consistent field (SCF) tolerance was 1×10^{-5} eV. The Brillouin zone was sampled by the Monkhorst-Pack scheme with a 4×4×1 k-points mesh for all of the surfaces. All the models were modelled with 4*4 supercell and a vacuum width of 10 Å was added in the z axis. For all the optimization calculations, the bottom one layers were fixed while the topmost two layers and the adsorbates were allowed to relax. The binding energies of H* were determined by the following formula $\Delta E_{H*} = E(\text{surf} + \text{H}) - E(\text{surf}) - 1/2E(\text{H}_2)$. The binding energies of OH* were determined by the following formula $\Delta E_{OH*} = E(\text{surf} + \text{OH}) - E(\text{surf}) - E(\text{H}_2\text{O}) + 1/2E(\text{H}_2)$.

$E_{sub\text{-}H}$ and $E_{sub\text{-}OH}$ represent total energies of the model with hydrogen and hydroxyl adsorption. E_{sub} represents total energy of the model. E_{H2} and E_{H2O} represent the energy of molecular H_2 and H_2O in gas phase.

The Gibbs free energy of H* adsorption was calculated as follows:

$\Delta G_{H*} = \Delta E_{H*} + \Delta ZPE - T\Delta S$

ΔZPE and ΔS represent the zero point energy correction and entropy change of hydrogen adsorption, respectively. And We refer to the previous work for the related values. [9]

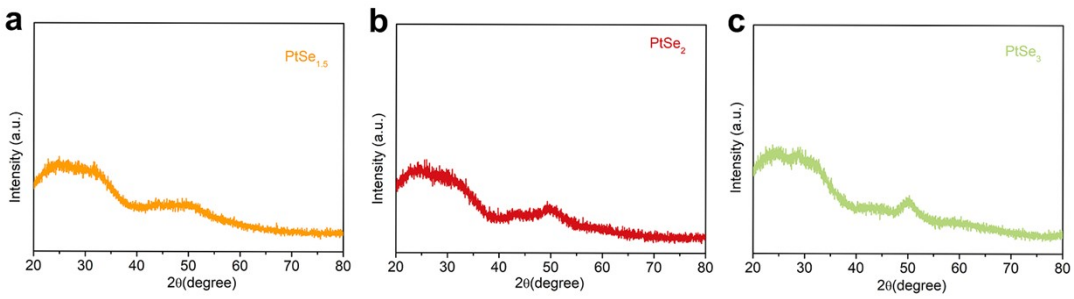

Figure S1 The XRD patterns of $PtSe_{1.5}$(a), $PtSe_2$(b) and $PtSe_3$(c).

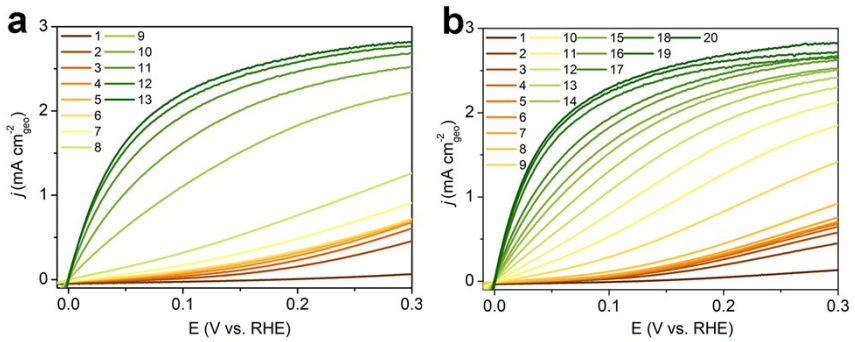

Figure S2 The activation process of $PtSe_{1.5}$(a) and $PtSe_3$(b) under the different HOR polarization scans

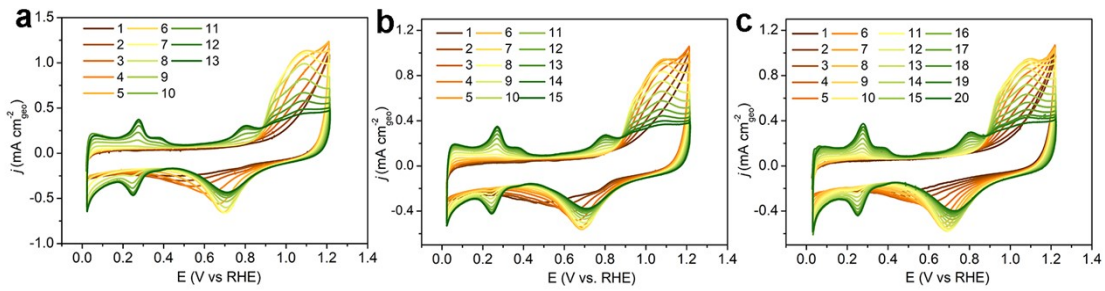

Figure S3 The activation process of $PtSe_{1.5}$(a), $PtSe_2$(b) and $PtSe_2$(c) under the different CV scans.

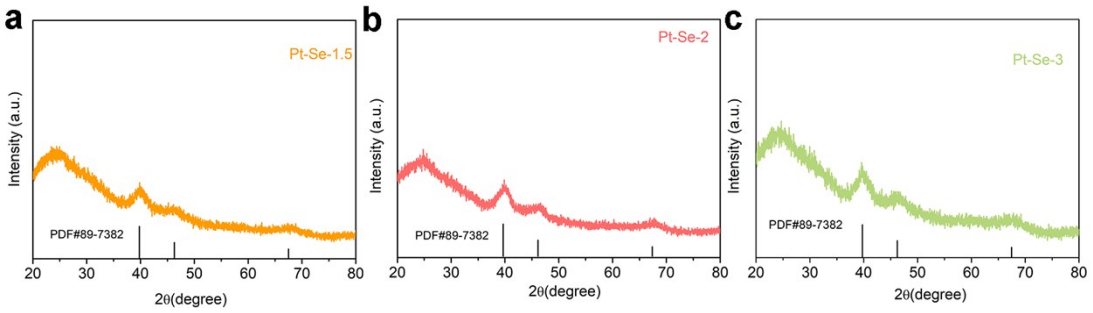

Figure S4 The XRD patterns of Pt-Se-1.5(a), Pt-Se-2(b) and Pt-Se-3(c).

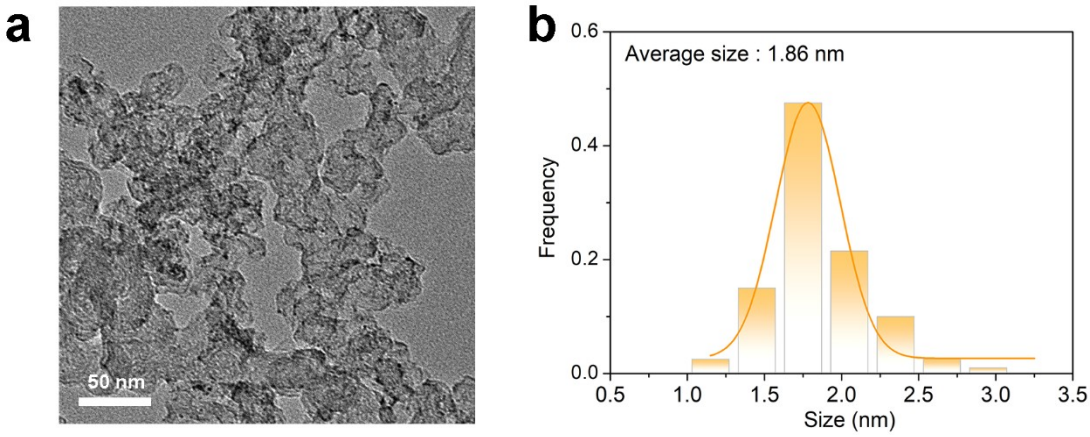

Figure S5 TEM image (a) and the corresponding size distribution (b) of $PtSe_2$.

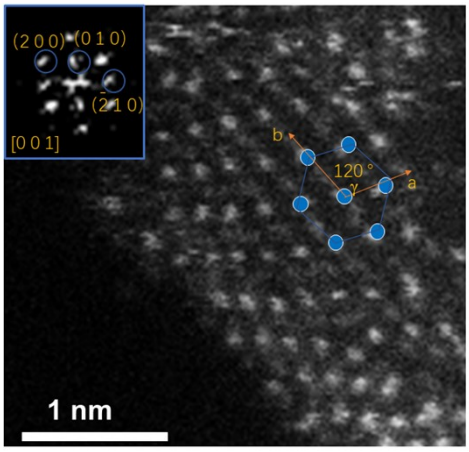

Figure S6 The atomic-resolution HAADF-STEM image of $PtSe_2$ and the corresponding FFT.

The blue ball presented the Pt atoms in the figure is arranged as the hexagon in the plane, indicating the obtained the six-fold rotation axis. The lattice edge lengths of a and b in the figure is same and the angle (γ) between a and b is 120 degrees. Combining with the lattice parameters and the high-order rotational symmetry, it can confirm that the $PtSe_2$ presents as the hexagonal crystal system. Besides, the corresponding FFT is inserted in the Figure S6. The signed diffraction spot can be assigned to the (200), (010) and (10), attributing to the [001] crystallographic direction of hcp $PtSe_2$.

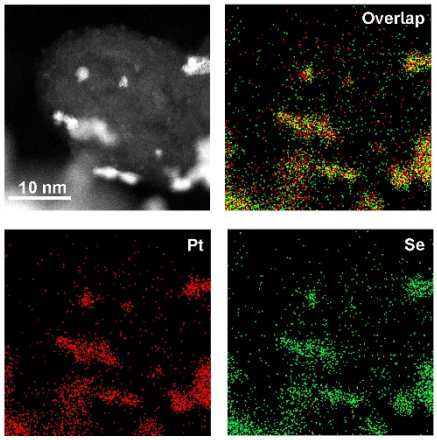

Figure S7 The EDX mappings of $PtSe_2$.

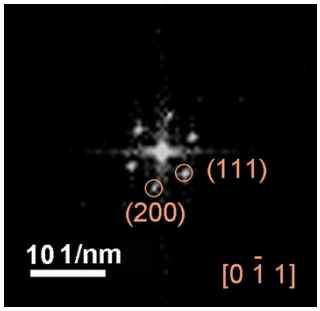

Figure S8 FFT of Pt-Se-2 from STEM images.

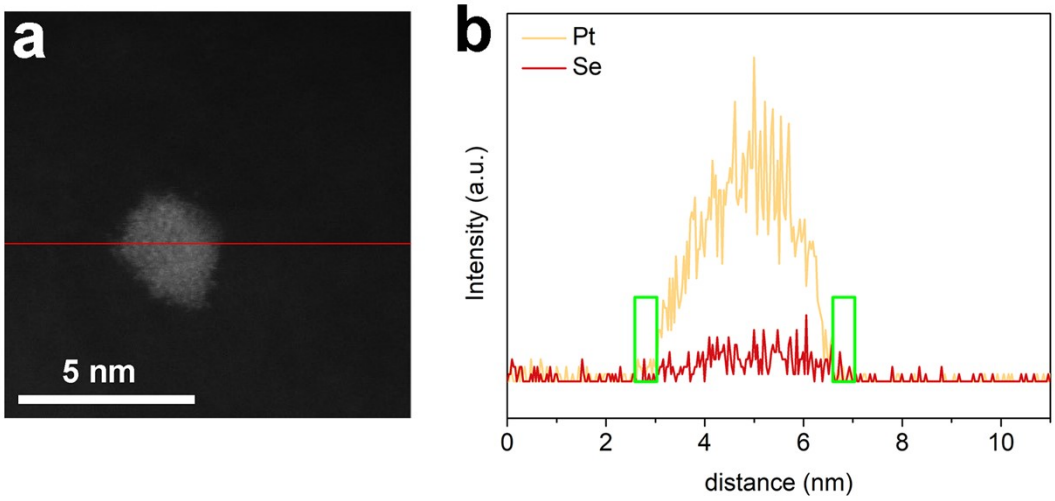

Figure S9 EDS line-scanning profile of a single Pt-Se-2.

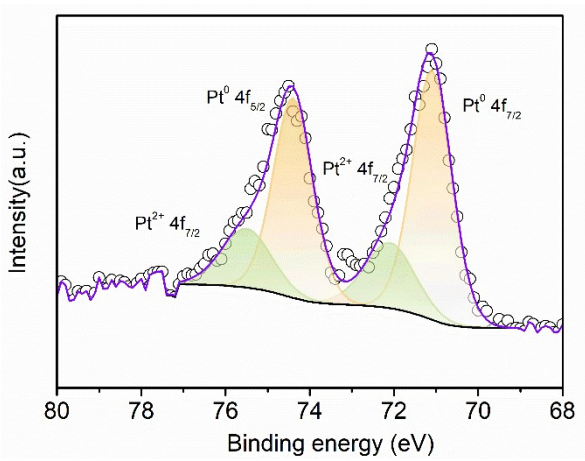

Figure S10 XPS spectra of Pt 4f in Pt.

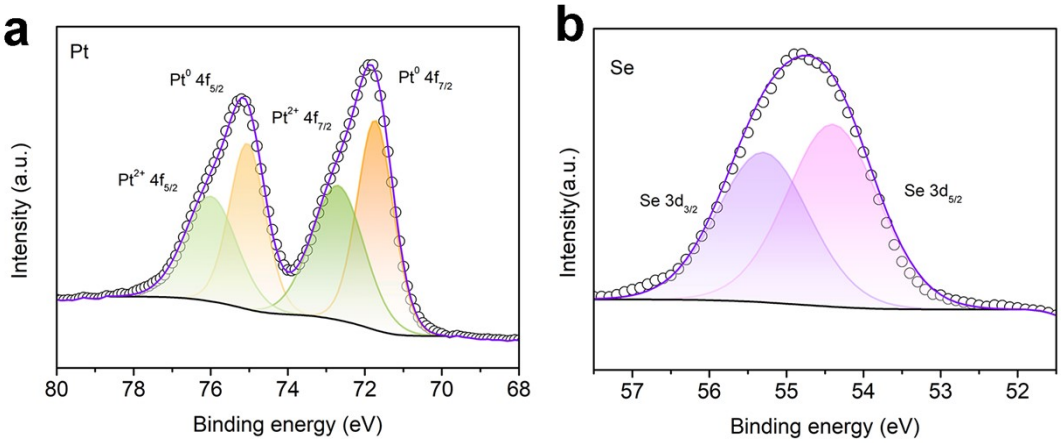

Figure S11 XPS spectra of Pt 4f (a) and Se 3d (b) for $PtSe_2$.

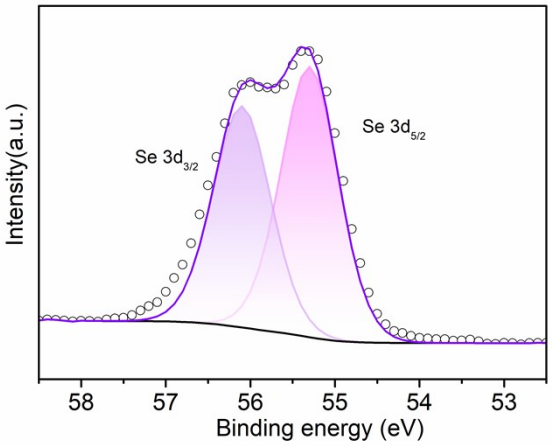

Figure S12 XPS spectra of Se 3d in Se powder.

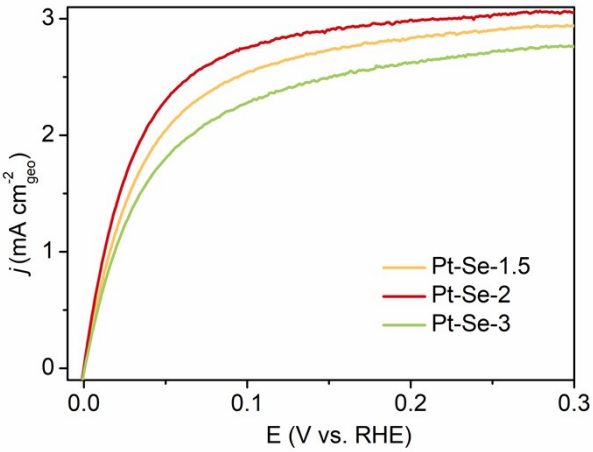

Figure S13 The HOR polarization curves of Pt-Se-x (x=1.5, 2 and 3) at the rotating speed of 1600 rpm with a scan rate of 10 mV s^{-1} in H_2-saturated 0.1 M KOH.

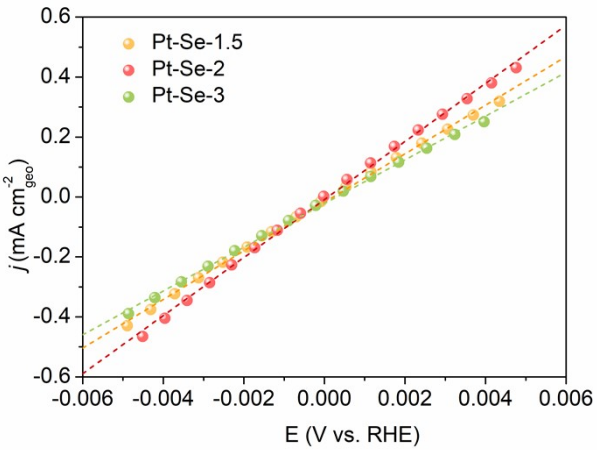

Figure S14 Linear-fitting curves in the micro-polarization region of HOR polarization curves of Pt-Se-x (x=1.5, 2 and 3).

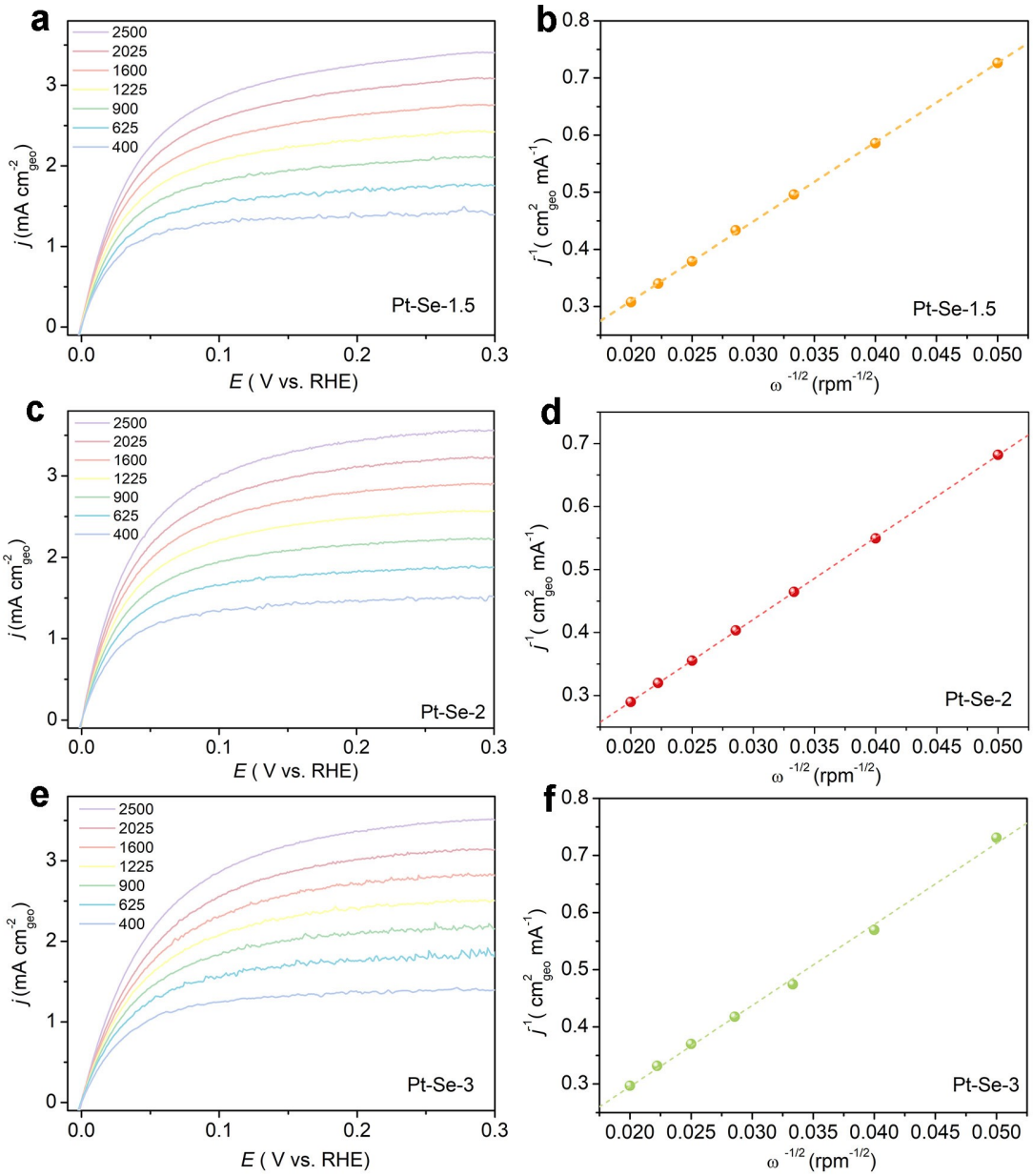

Figure S15 Polarization curves of Pt-Se-1.5 (a), Pt-Se-2 (c) and Pt-Se-3 (e) in H_2-saturated 0.1 M KOH solution at the rotating speeds varied from 2500 to 400 rpm. And the Koutecky–Levich plot of Pt-Se-1.5 (b), Pt-Se-2 (d) and Pt-Se-3 (f).

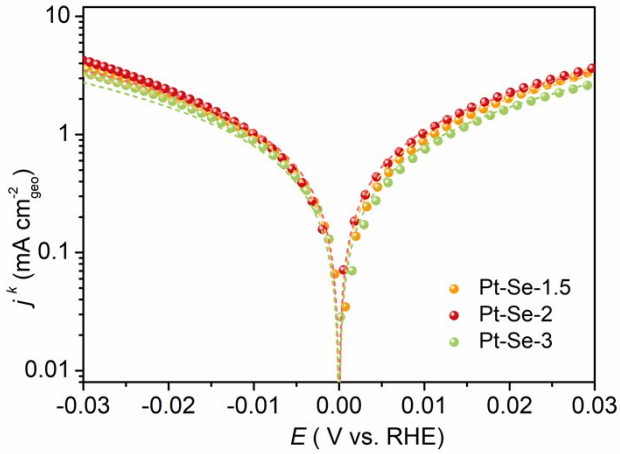

Figure S16 Tafel plots with the Butler–Volmer fitting lines of Pt-Se-x (x=1.5, 2 and 3)

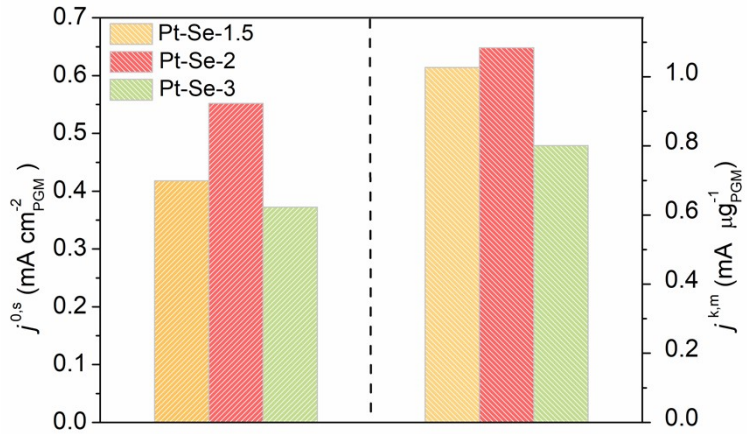

Figure S17 Comparison of the specific activities($j^{0,s}$) and the mass activities ($j^{k,m}$)(@ 50 mV) of Pt-Se-x (x=1.5, 2 and 3)

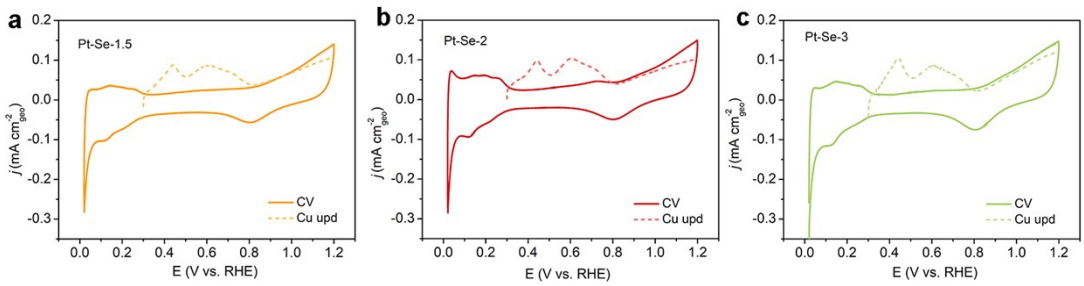

Figure S18 The CV curves of Pt-Se-1.5 (a), Pt-Se-2 (b) and Pt-Se-3 (c) as well as the Cu-UPD zones.

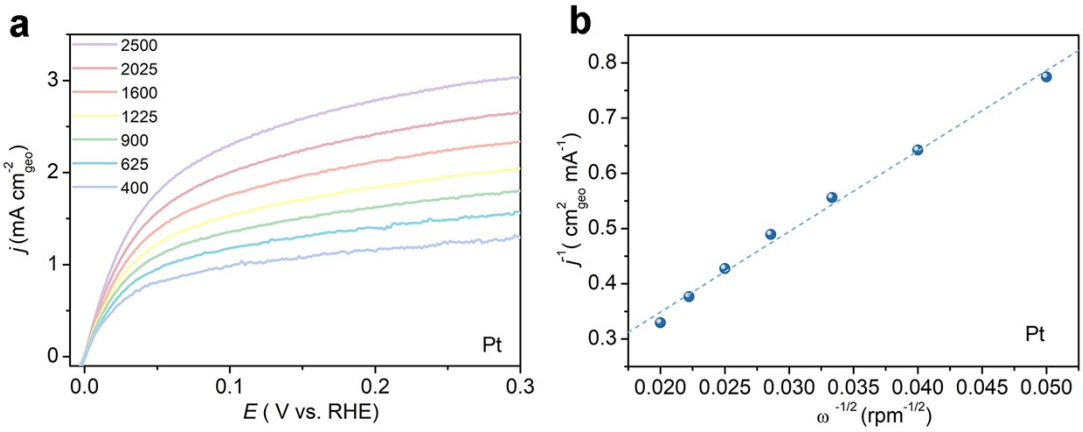

Figure S19 Polarization curves of Pt (a) in H_2-saturated 0.1 M KOH solution at the rotating speeds varied from 2500 to 400 rpm. And the Koutecky–Levich plot of Pt (b).

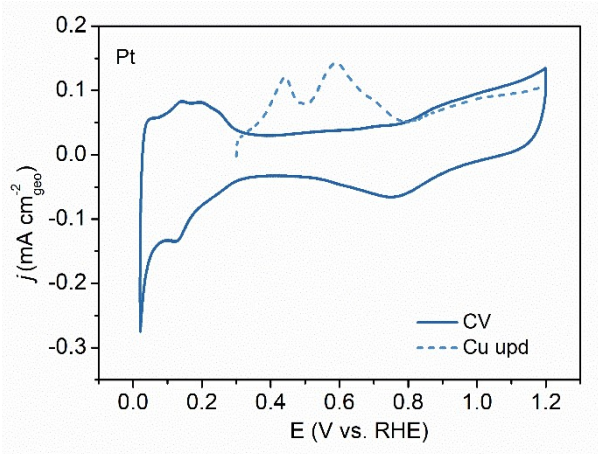

Figure S20 The CV curves of Pt as well as the Cu-UPD zones.

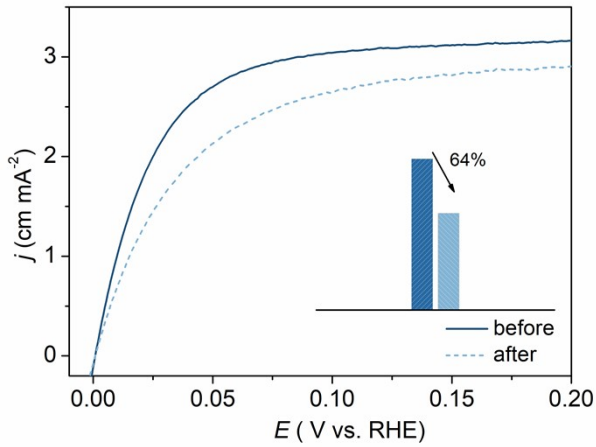

Figure S21 HOR polarization curves of Pt in H_2-saturated 0.1 M KOH at a rotating speed of 1600 rpm before and after 1000 CVs.

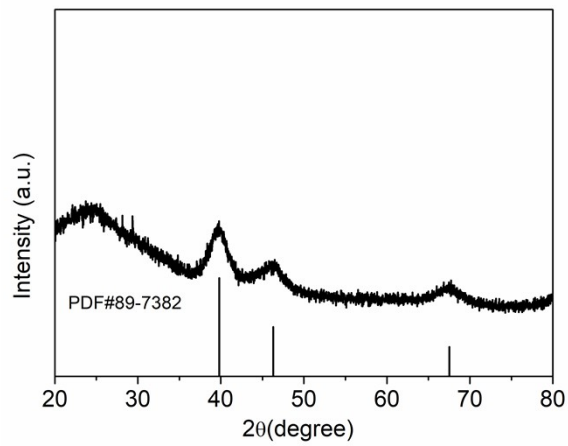

Figure S22 The XRD patterns of Pt-Se-2 after the stability test.

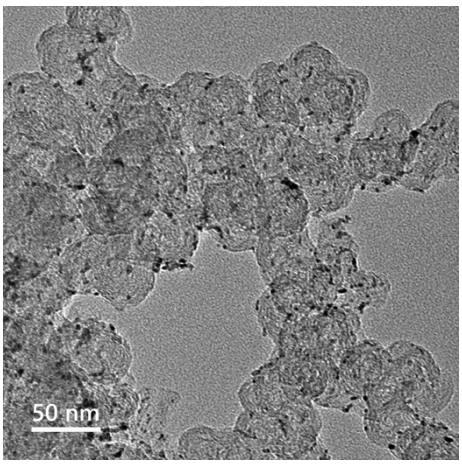

Figure S23 TEM image of Pt-Se-2 after the stability test.

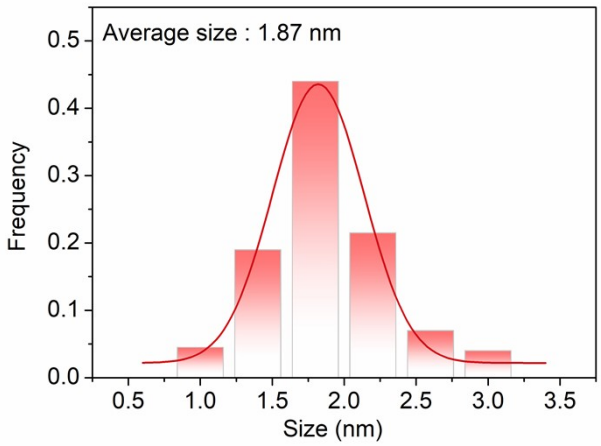

Figure S24 The corresponding size distribution of Pt-Se-2 after stability test.

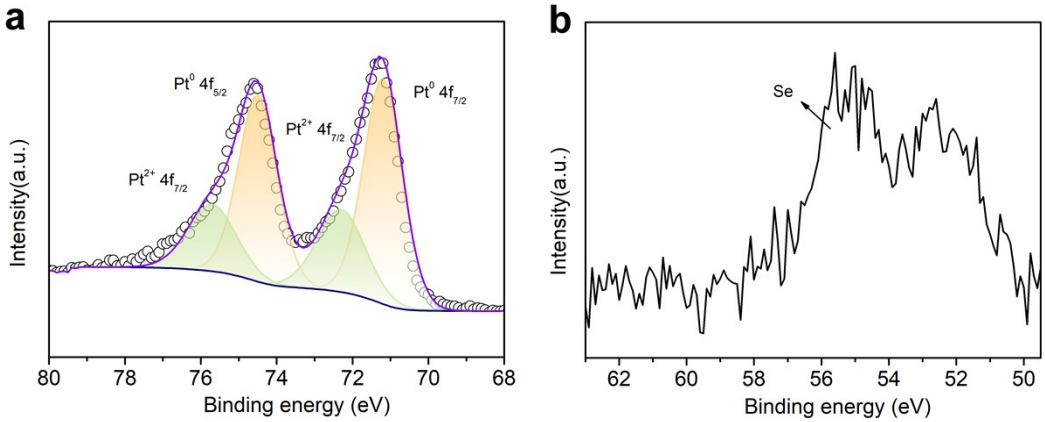

Figure S25 XPS pattern of Pt and Se of Pt-Se-2 after the stability test.

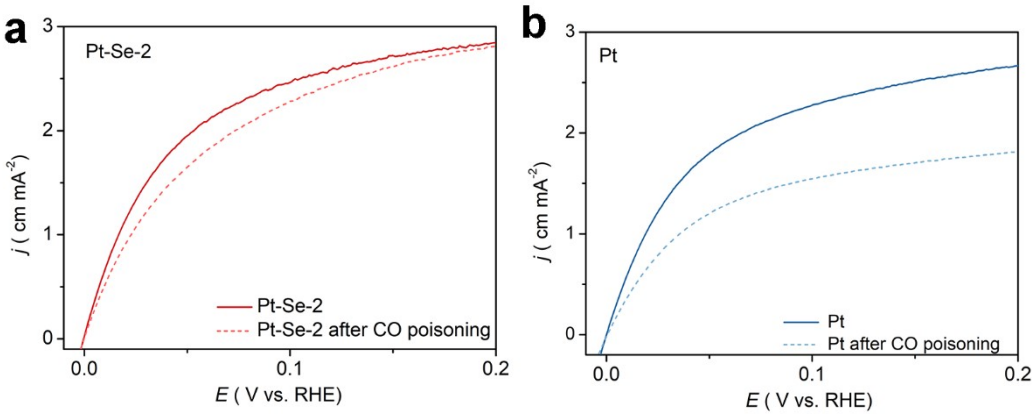

Figure S26 Comparison of the HOR curves of Pt-Se-2 (a) and commercial Pt (b) in H_2-saturated 0.1 M KOH before (solid line) and after (dash line) the chronoamperometry test with 100 ppm CO (CO poisoning test).

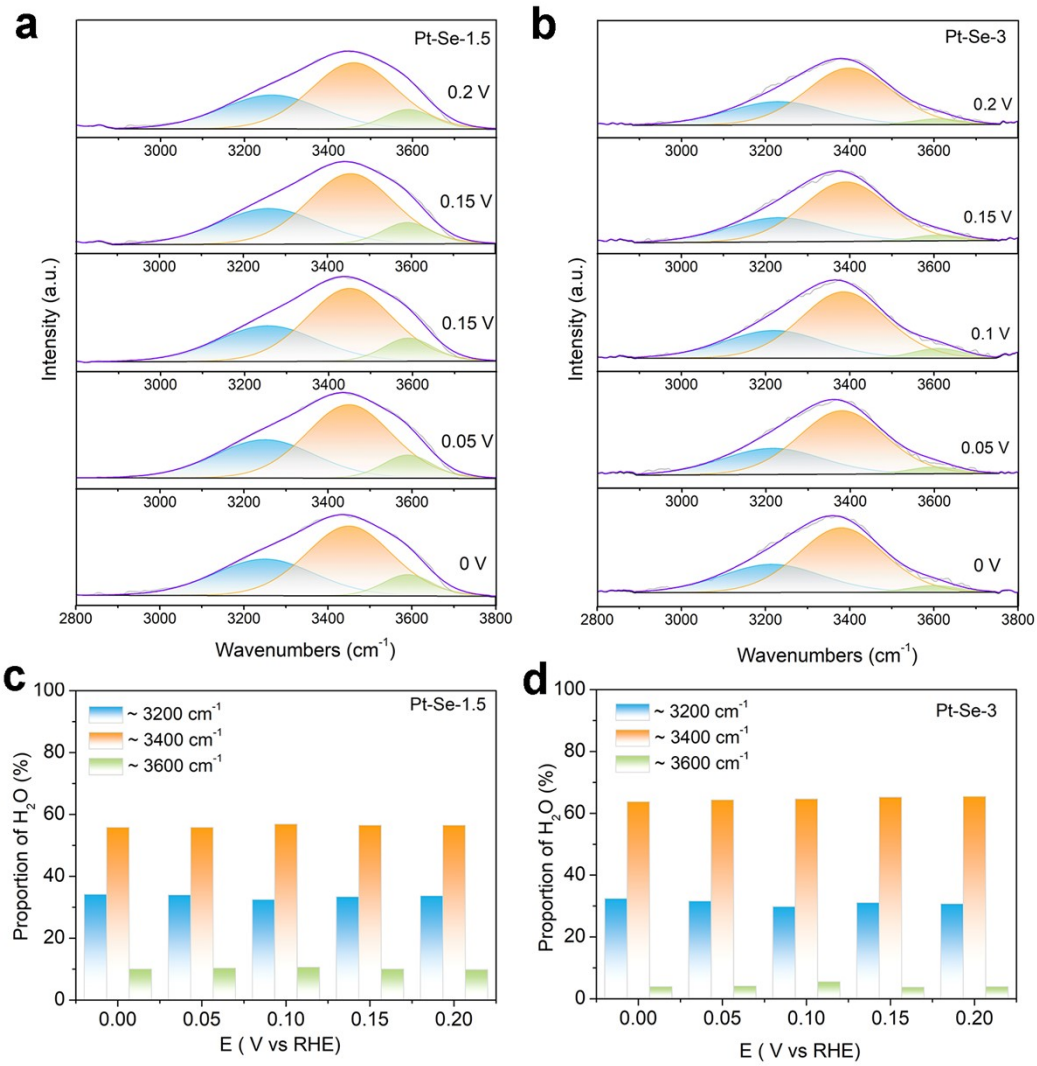

Figure S27 Deconvolution of the O-H stretching vibration features of in situ SEIRAS spectra recorded at potentials from 0 V to 0.2 V vs RHE for Pt-Se-1.5 (a) and Pt-Se-3 (b) in 0.1 M KOH. The proportion of the three kinds of water molecules from the deconvolution of the O-H stretching vibration features of Pt-Se-1.5 (c) and Pt-Se-3 (d)

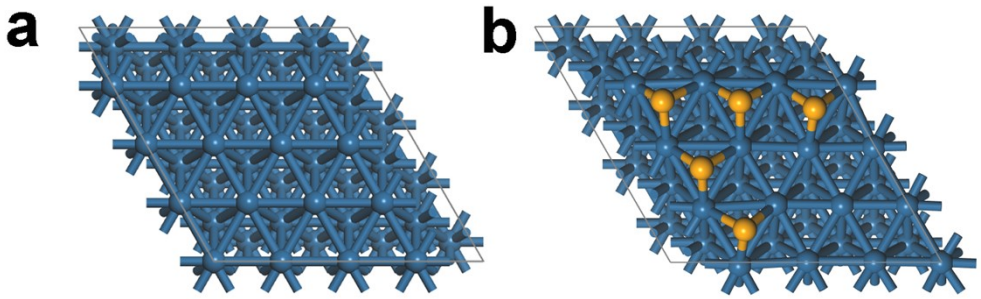

Figure S28 The geometric configurations of Pt (a) and Pt-Se-2 (b)

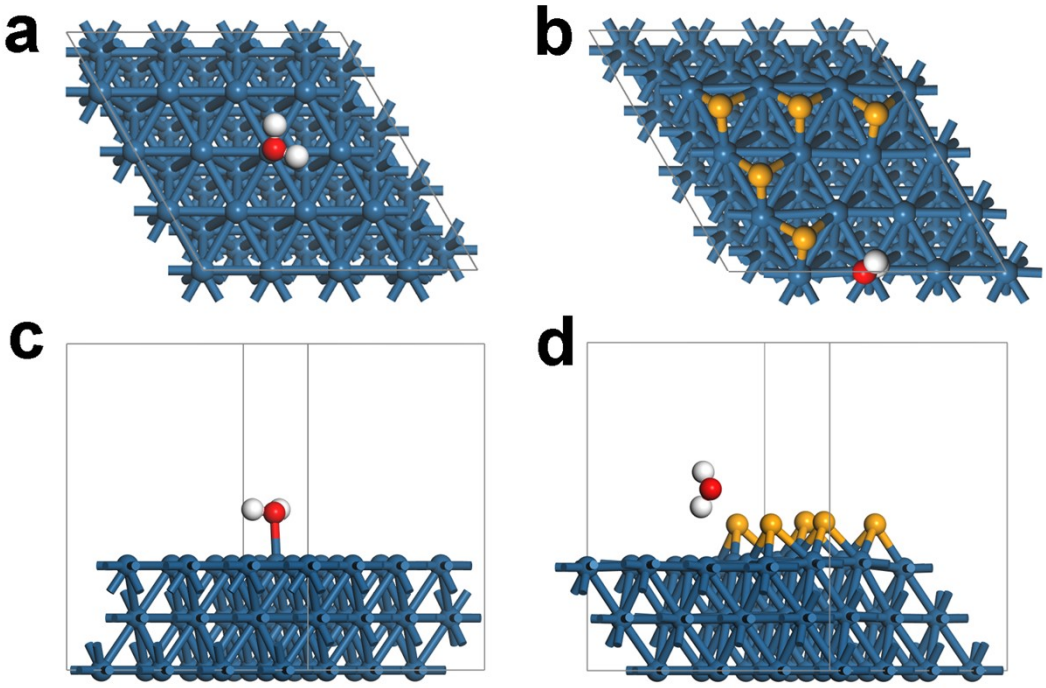

Figure S29 The optimal theoretical structures of H_2O adsorbed on Pt (a) and the corresponding side view (c) and Pt-Se-2 (b) and the corresponding side view (d).

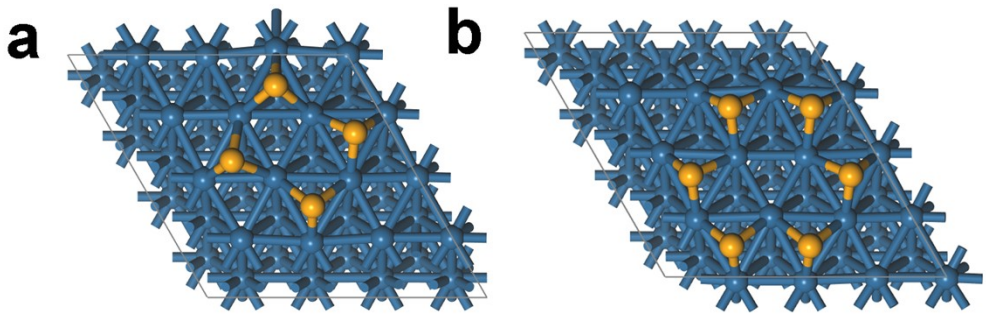

Figure S30 The geometric configurations of Pt-Se-1.5 (a) and Pt-Se-3 (b)

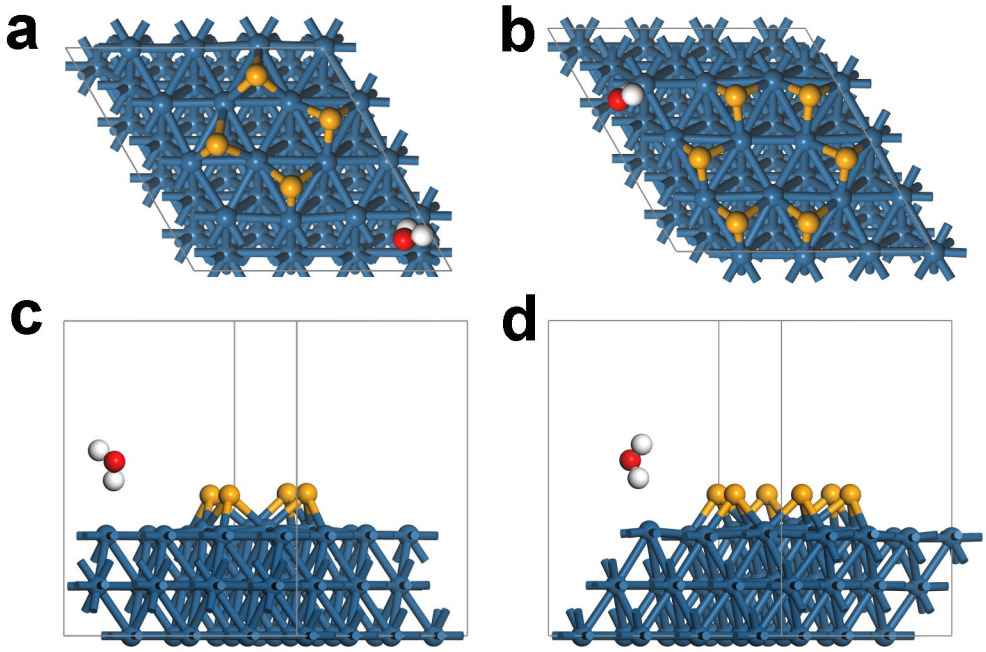

Figure S31 The optimal theoretical structures of H_2O adsorbed on Pt-Se-1.5 (a) and the corresponding side view (c) and Pt-Se-3 (b) and the corresponding side view (d).

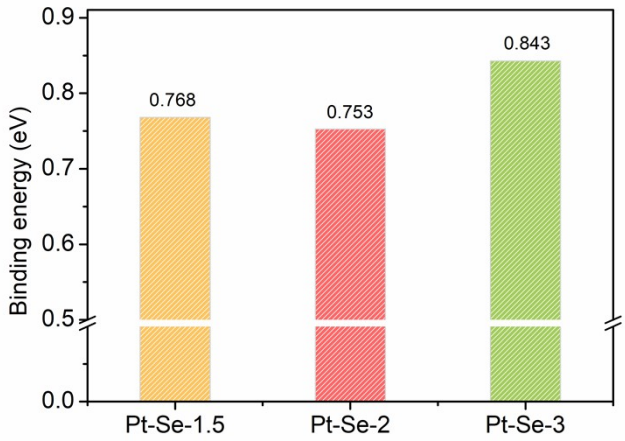

Figure S32 The adsorption energy of OH* on Pt-Se-x(x=1.5,2,3)

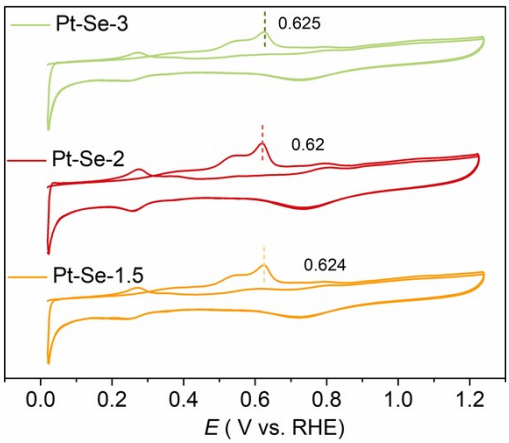

Figure S33 CO stripping curves of Pt-Se-x (x=1.5,2,3) in CO-statured 0.1 M KOH.

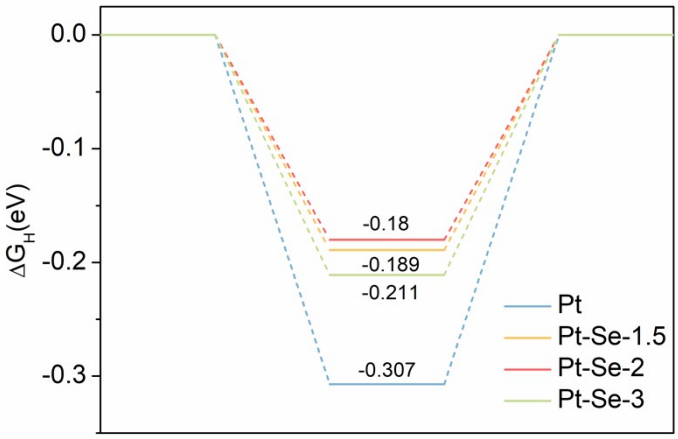

Figure S34 The adsorption energy of H* on Pt-Se-x(x=1.5,2,3) and Pt.

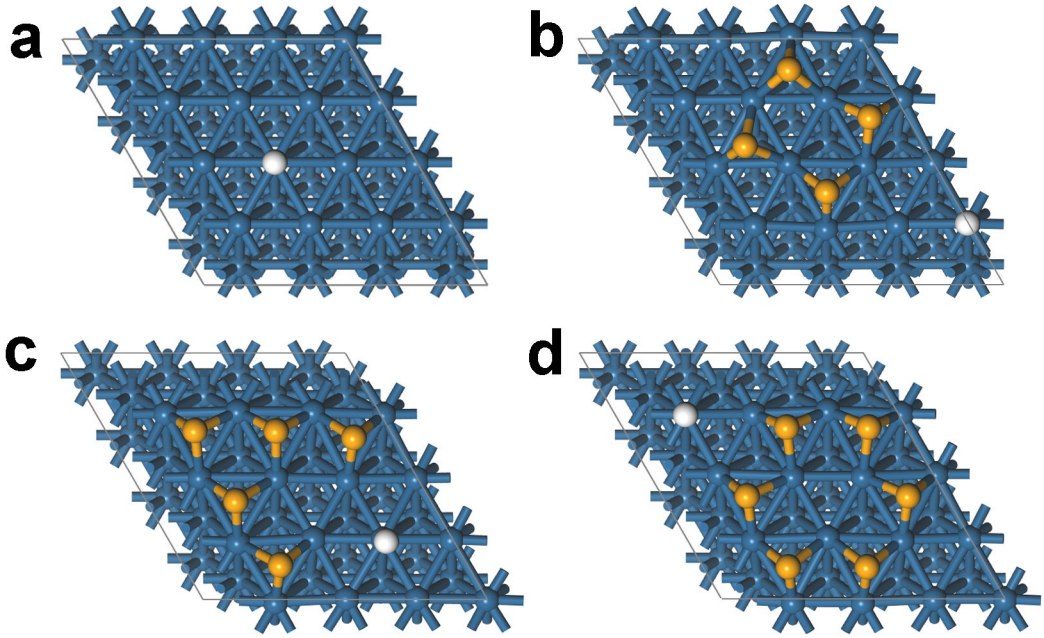

Figure S35 The optimal theoretical structures of H adsorbed on Pt (a), Pt-Se-1.5 (b), Pt-Se-2 (c) and Pt-Se-3 (d).

Table S1 ICP-AES results of the contents of Se and Pt in different catalysts.

Catalyst	Pt (wt. %)	Se (wt. %)	Atomic Ratio(Se/Pt)
$PtSe_2$	14.9	11.4	1.90
Pt-Se-2	12.9	2.91	0.56
Pt-Se-1.5	13.2	2.48	0.46
Pt-Se-3	13.4	4.29	0.72

Table S2 XPS results of the contents of Se and Pt in different catalysts.

Catalyst	Pt (Atomic %)	Se (Atomic %)	Atomic Ratio(Se/Pt)
Pt-Se-2	1.24	1.32	0.92

Table S3. HOR activities of the reported PGM-based catalysts in alkaline media.

Catalyst	Loading (μg_{PGM} cm^{-2})	$j^{0,s}$ (mA cm_{metal}^{-2})	$j^{k,m}$@50 mV (mA μg_{metal}^{-1})	Reference
Pt-Se-2	7.59	0.552	1.084	This work
O-RuNi@C-400	13.84	/	0.601	10
Ru/Meso C	25.4	/	0.54	11
Rh NBs	10	0.146	0.361	11
Ru-TiO_2/C	25.48	0.15	0.097	12
Ru/C	25.48	0.12	0.052	12
$Ru_{0.7}Ni_{0.3}$/C	14	0.13	0.14	13
$Ru_{0.95}Fe_{0.05}$/C	14	0.11	0.16	13
$(Pt_{0.9}Pd_{0.1})_3Fe$/C	5	0.305	/	14
Ru-Ir(2/3)/C	10	0.283	0.210	15
Ru/PEI-XC	21.7	0.687	0.423	16
20% Pt/C	20.4	0.2	0.385	16
D-Pt_3In	10	/	0.934	17

RuRh-Co	5	1.91	11.7	18
PtRu/Mo_2C-TaC	13	0.2	0.291	19
Ir/α-MoC_{1-x}		0.455	0.445	20
Ru colloidosomes	57	0.045	/	21
$Pb_{1.04}$-$Ru_{92}Cu_8$ NFs/C	1.8	/	1.10	22
Rh NSs	56	0.258	0.32	23
Rh-GB NSs	56	0.343	0.37	23
Ni_1Ru_1/C(L)	12.5	0.078	0.224	24
Ni_1Ru_1/C(H)	49.9	0.030	0.116	24
Sub-2 nm Ru/HC	14.7	/	0.30	25
Sub-2 nm RuMo/HC	13.3	/	3.83	25
PtMo NPs/C	~9.43	0.63	0.805	26
PtMo/MoO_{x-1}/C	~9.43	0.83	3.19	26
Ru@C-400	10	0.31	0.64	27
Pd_3Co@Pt/C	1.87	0.57	0.685	28
Rh_2Sb NBs	6.38	0.51	0.462	29
Pt_3Ni NWs/C	15.3	0.31	0.77	30
Ir NW/C	7.65	0.429	0.641	31
Ir_4Sb NW/C	7.65	0.949	2.23	31
Pt-MoC@NC	10	0.560	0.833	32
$Pt_{0.25}Ru_{0.75}$/N-C	50	1.41	1.654	33
Pt-Sn-Sb	10	/	2.55	34
Ir/MoS_2-RT	200	0.74	/	35
a-$Pt_{53}Ru_{47}$	10.2	1.9	13.7@25 mV	36
$PtRu_3$/PC	4	1.312	11.24	37

Au_1Pt_2/C	3.5	0.51	0.06	38
$Co_{0.2}Ru_{0.7}Pt_{0.1}$/PNC NSs	5	4.28	1.84	39
D-IrFe/C	3.94	/	0.784	40
di-RuNi MLNS/C	3	/	1.79	41
hcp RuNi	28	1.95	0.0818	42
HEA-PdNiRuIrRh NPs	6.98	1.19	3.247	43
Ir/Ni-NiO/CNT	29.46	2.04	1.59	44
Ir/α-W	/	0.89	/	45
Ir/β-W	/	0.49	/	45
$Ir_1Pd_1Ru_8$/C	3.5	0.24	0.15@10 mV	46
Ir_1Ru_3NWs/C	29	0.0838	3.346	47
$IrMo_{0.59}$ NPs	1.75	1.15	3.85	48
IrNi@Ir/C	10	1.22	1.12	49
IrNi@PdIr/C	19.7	0.209	0.854	50
La_1Pt@HCS	10	1.55	/	51
metallic Pd	~15	0.34	/	52
Mo-Pt/NC	10	11.76	4.549	53
Mo-Ru NSAs	/	/	2.45	54
Mo-Ru-2/C	6	0.35	1.86	55
NiIr(BCS)/GO	31.8	/	0.33	56
O-PdFe@Pt	7.05	/	0.658	57
Pd/CuNWs	18	0.33	/	58
$Pd_{0.10}Ru_{0.80}Mo_{0.10}$/C	10	/	0.896	59
Pd_9Ag_1/C	10	0.033	/	60

PdO-RuO_2/C	40	0.512	0.221	61
Pd-Pd_4S/C	/	0.224	0.013@10 mV	62
Pt_2IrDNWs/C	10.2	/	3.48	63
Pt_2-Rh NSs	15.3	2.07	9.61	64
Pt_7Ru_3/C	3.5	1.11	0.49@100 mV	65
$Pt_{8.7}$-RuCu	/	/	5.91	66
$PtNi_2$-CDs/C	5	3.33	10.16	67
PtNi-S	10	6.58	4.08	68
$PtPdCu_1$/C	/	/	0.6	69
PtRh NAA	25.5	0.45	0.49	70
PtRhMoIrRu-HEA NWs	9.1	/	5.8	71
$PtRu_{0.6}$/NC	8.5	3.2	3.08	72
PtRuNiCoFeMo HEA SNWs	8.8	0.753	6.75	73
PtRu-NWs	20	0.493	2.2	74
$PtSb_2$@Pt	0.83	0.78	/	75
Rh_2P/C	6.4	0.65	/	76
Rh_2Sb NBs	5	0.305	/	77
RhMo NSs	17.6	/	6.96	78
RhSn/C	/	0.933	/	79
Ru/RuO_2	/	0.466	/	80
$Ru_{0.20}Pd_{0.80}$	7.06	0.148	0.138	81
Ru_1Ptn SAA	4	1.992	4.71	82
Ru_2Ni MLNSs	/	/	4.34	83
Ru2P	10	0.37	/	84
Ru_3Sn_7/C	10	0.506	/	85
Ru_7Ni_3/C	0.76	/	7.1	86
RuCr-2/C	4.5	0.399	0.586	87

$RuFe_{0.1}/C$	1.25	0.544	0.934	88
Ru-MnO/C	20	/	0.78	89
$RuNi_1$	8.8		2.7	90
RuO_2-PdO/C	11.3	/	1.5	91
RuP/NOC	18.1	/	3.25	92
RuPdIr/C	/	0.53	/	93
Ru-Ru_2P/C	8.33	/	1.265	94
Ga-Ru/C	7.04	0.3	0.593	95
Sn-Ru/C	6.26	0.47	1.79	95

References

1. Cong, Y. Y.; Yi, B. L.; Song, Y. J., Hydrogen oxidation reaction in alkaline media: From mechanism to recent electrocatalysts. *Nano Energy* **2018,** *44*, 288-303.
2. Sheng, W. C.; Gasteiger, H. A.; Shao-Horn, Y., Hydrogen Oxidation and Evolution Reaction Kinetics on Platinum: Acid vs Alkaline Electrolytes. *J. Electrochem. Soc.* **2010,** *157* (11), B1529-B1536.
3. Zheng, J.; Zhuang, Z. B.; Xu, B. J.; Yan, Y. S., Correlating Hydrogen Oxidation/Evolution Reaction Activity with the Minority Weak Hydrogen-Binding Sites on Ir/C Catalysts. *ACS Catal.* **2015,** *5* (7), 4449-4455.
4. Durst, J.; Siebel, A.; Simon, C.; Hasché, F.; Herranz, J.; Gasteiger, H. A., New insights into the electrochemical hydrogen oxidation and evolution reaction mechanism. *Energy Environ. Sci.* **2014,** *7* (7), 2255-2260.
5. Ohyama, J.; Sato, T.; Yamamoto, Y.; Arai, S.; Satsuma, A., Size Specifically High Activity of Ru Nanoparticles for Hydrogen Oxidation Reaction in Alkaline Electrolyte. *J. Am. Chem. Soc.* **2013,** *135* (21), 8016-8021.
6. Duan, Y.; Yu, Z. Y.; Yang, L.; Zheng, L. R.; Zhang, C. T.; Yang, X. T.; Gao, F. Y.; Zhang, X. L.; Yu, X. X.; Liu, R.; Ding, H. H.; Gu, C.; Zheng, X. S.; Shi, L.; Jiang, J.; Zhu, J. F.; Gao, M. R.; Yu, S. H., Bimetallic nickel-molybdenum/tungsten nanoalloys for high-efficiency hydrogen oxidation catalysis in alkaline electrolytes. *Nat. Commun.* **2020,** *11* (1), 4789.
7. Perdew, J. P.; Burke, K.; Ernzerhof, M., Generalized gradient approximation made simple (vol 77, pg 3865, 1996). *Phys. Rev. Lett.* **1997,** *78* (7), 1396-1396.
8. Hammer, B.; Hansen, L. B.; Norskov, J. K., Improved adsorption energetics within density-functional theory using revised Perdew-Burke-Ernzerhof functionals. *Phys. Rev. B* **1999,** *59* (11), 7413-7421.
9. Norskov, J. K.; Bligaard, T.; Logadottir, A.; Kitchin, J. R.; Chen, J. G.; Pandelov, S.; Norskov, J. K., Trends in the exchange current for hydrogen evolution. *J. Electrochem. Soc.* **2005,** *152* (3), J23-J26.

10. Zhang, X. J.; Li, Z. Q.; Sun, X. P.; Wei, L. Z.; Niu, H. L.; Chen, S.; Chen, Q. W.; Wang, C. L.; Zheng, F. C., Regulating the Surface Electronic Structure of RuNi Alloys for Boosting Alkaline Hydrogen Oxidation Electrocatalysis. *ACS Mater. Lett.* **2022,** *4* (11), 2097-2105.
11. Jiang, J. X.; Tao, S. C.; He, Q.; Wang, J.; Zhou, Y. Y.; Xie, Z. Y.; Ding, W.; Wei, Z. D., Interphase-oxidized ruthenium metal with half-filled d-orbitals for hydrogen oxidation in an alkaline solution. *J. Mater. Chem. A* **2020,** *8* (20), 10168-10174.
12. Zeng, L. M.; Peng, H. Q.; Liu, W.; Yin, J. L.; Xiao, L.; Lu, J. T.; Zhuang, L., Extraordinary activity of mesoporous carbon supported Ru toward the hydrogen oxidation reaction in alkaline media. *J. Power Sources* **2020,** *461*, 228147.
13. Wang, H. S.; Yang, Y.; DiSalvo, F. J.; Abruña, H. D., Multifunctional Electrocatalysts: Ru-M (M = Co, Ni, Fe) for Alkaline Fuel Cells and Electrolyzers. *ACS Catal.* **2020,** *10* (8), 4608-4616.
14. Zhao, T. H.; Wang, G. J.; Gong, M. X.; Xiao, D. D.; Chen, Y.; Shen, T.; Lu, Y.; Zhang, J.; Xin, H. L.; Li, Q.; Wang, D. L., Self-Optimized Ligand Effect in L1₂-PtPdFe Intermetallic for Efficient and Stable Alkaline Hydrogen Oxidation Reaction. *ACS Catal.* **2020,** *10* (24), 15207-15216.
15. Ishikawa, K.; Ohyama, J.; Okubo, K.; Murata, K.; Satsuma, A., Enhancement of Alkaline Hydrogen Oxidation Reaction of Ru-Ir Alloy Nanoparticles through Bifunctional Mechanism on Ru-Ir Pair Site. *ACS Appl. Mater. Interfaces* **2020,** *12* (20), 22771-22777.
16. Wang, J.; Liu, J.; Zhang, B. Y.; Gao, J.; Liu, G. B.; Cui, X. J.; Liu, J. X.; Jiang, L. H., Amine-ligand modulated ruthenium nanoclusters as a superior bi-functional hydrogen electrocatalyst in alkaline media. *J. Mater. Chem. A* **2021,** *9* (40), 22934-22942.
17. Wu, J.; Gao, X.; Liu, G. M.; Qiu, X. Y.; Xia, Q.; Wang, X. Z.; Zhu, W. X.; He, T. W.; Zhou, Y. J.; Feng, K.; Wang, J. X.; Huang, H.; Liu, Y.; Shao, M. H.; Kang, Z. H.; Zhang, X., Immobilizing Ordered Oxophilic Indium Sites on Platinum Enabling Efficient Hydrogen Oxidation in Alkaline Electrolyte. *J. Am. Chem. Soc.* **2024,** *146* (29), 20323-20332.
18. Cui, Y. J.; Xu, Z. H.; Chen, D.; Li, T. T.; Yang, H.; Mu, X. Q.; Gu, X. Y.; Zhou, H.; Liu, S. L.; Mu, S. C., Trace oxophilic metal induced surface reconstruction at buried RuRh cluster interfaces possesses extremely fast hydrogen redox kinetics. *Nano Energy* **2021,** *90*, 106579.
19. Hamo, E. R.; Singh, R. K.; Douglin, J. C.; Chen, S. A.; Ben Hassine, M.; Carbo-Argibay, E.; Lu, S. F.; Wang, H. N.; Ferreira, P. J.; Rosen, B. A.; Dekel, D. R., Carbide-Supported PtRu Catalysts for Hydrogen Oxidation Reaction in Alkaline Electrolyte. *ACS Catal.* **2021,** *11* (2), 932-947.
20. Han, Y. C.; Zhao, L.; Cheng, W.; Wang, M. Z.; Yang, L.; Lin, Y. X.; Xu, K., Iridium Cluster Anchored onto Cubic Molybdenum Carbide with Strong Electronic Interactions for Robust Hydrogen Oxidation Reaction in Alkaline Medium. *Adv. Funct. Mater.* **2024,** *34* (44), 2407060.

21. Yang, X. D.; Ouyang, B.; Shen, P. Q.; Sun, Y. Q.; Yang, Y. S.; Gao, Y. A.; Kan, E. J.; Li, C. C.; Xu, K.; Xie, Y., Ru Colloidosome Catalysts for the Hydrogen Oxidation Reaction in Alkaline Media. *J. Am. Chem. Soc.* **2022,** *144* (25), 11138-11147.
22. Dong, Y. T.; Zhang, Z. M.; Yan, W.; Hu, X. R.; Zhan, C. H.; Xu, Y.; Huang, X. Q., Pb-Modified Ultrathin RuCu Nanoflowers for Active, Stable, and CO-resistant Alkaline Electrocatalytic Hydrogen Oxidation. *Angew. Chem.-Int. Edit.* **2023,** *62* (44), e202311722.
23. Yang, X. D.; Ouyang, B.; Zhao, L.; Shen, Q.; Chen, G. Z.; Sun, Y. Q.; Li, C. C.; Xu, K., Ultrathin Rh Nanosheets with Rich Grain Boundaries for Efficient Hydrogen Oxidation Electrocatalysis. *J. Am. Chem. Soc.* **2023,** *145* (49), 27010-27021.
24. Liu, J.; Wang, J.; Fo, Y.; Zhang, B. Y.; Molochas, C.; Gao, J.; Li, W. Z.; Cui, X. J.; Zhou, X.; Jiang, L. H.; Tsiakaras, P., Engineering of unique Ni-Ru nano-twins for highly active and robust bifunctional hydrogen oxidation and hydrogen evolution electrocatalysis. *Chem. Eng. J.* **2023,** *454*, 139959.
25. Ma, M.; Chen, C. F.; Zhang, X. B.; Zhao, H. S.; Wang, Q. X.; Du, G. F.; Xie, Z. X.; Kuang, Q., Mo-modified electronic effect on sub-2 nm Ru catalyst for enhancing hydrogen oxidation catalysis. *J. Mater. Chem. A* **2023,** *11* (20), 10807-10812.
26. Luo, H.; Wang, K.; Lin, F. X.; Lv, F.; Zhou, J. H.; Zhang, W. Y.; Wang, D. W.; Zhang, W. S.; Zhang, Q. H.; Gu, L.; Luo, M. C.; Guo, S. J., Amorphous MoO_x with High Oxophilicity Interfaced with PtMo Alloy Nanoparticles Boosts Anti-CO Hydrogen Electrocatalysis. *Adv. Mater.* **2023,** *35* (29), 2211854.
27. Yang, Z. L.; Lai, W. C.; He, B. L.; Wang, J.; Yu, F. F.; Liu, Q. H.; Liu, M. C.; Zhang, S. G.; Ding, W.; Lin, Z. Q.; Huang, H. W., Tailoring Interfacial Chemistry of Defective Carbon-Supported Ru Catalyst Toward Efficient and CO-Tolerant Alkaline Hydrogen Oxidation Reaction. *Adv. Energy Mater.* **2023,** *13* (26), 2300881.
28. Zhao, T. H.; Hu, Y. C.; Gong, M. X.; Lin, R. Q.; Deng, S. F.; Lu, Y.; Liu, X. P.; Chen, Y.; Shen, T.; Hu, Y. Z.; Han, L. L.; Xin, H. L.; Chen, S. L.; Wang, D. L., Electronic structure and oxophilicity optimization of mono-layer Pt for efficient electrocatalysis. *Nano Energy* **2020,** *74*, 104877.
29. Zhang, Y.; Li, G.; Zhao, Z. L.; Han, L. L.; Feng, Y. G.; Liu, S. H.; Xu, B. Y.; Liao, H. G.; Lu, G.; Xin, H. L.; Huang, X. Q., Atomically Isolated Rh Sites within Highly Branched Rh₂Sb Nanostructures Enhance Bifunctional Hydrogen Electrocatalysis. *Adv. Mater.* **2021,** *33* (43), 2105049.
30. Wang, L. Y.; Meng, S.; Tang, C. Y.; Zhan, C. H.; Geng, S. Z.; Jiang, K. Z.; Huang, X. Q.; Bu, L. Z., PtNi/PtIn-Skin Fishbone-Like Nanowires Boost Alkaline Hydrogen Oxidation Catalysis. *ACS Nano* **2023,** *17* (18), 17779-17789.
31. Xu, B. Y.; Huang, X.; Liu, S. H.; Hu, Z. W.; Kao, C. W.; Chan, T. S.; Geng, H. B.; Zhang, Y.; Huang, X. Q., Antimony oxides-protected ultrathin Ir-Sb

nanowires as bifunctional hydrogen electrocatalysts. *Nano Res.* **2024,** *17* (3), 1042-1049.

32. Zhou, F.; Ke, X. F.; Chen, Y. H.; Zhao, M.; Yang, Y.; Dong, Y. Q.; Zou, C.; Chen, X. A.; Jin, H. L.; Zhang, L. J.; Wang, S., Electron-distribution control via Pt/NC and MoC/NC dual junction: Boosted hydrogen electro-oxidation and theoretical study. *J. Energy Chem.* **2024,** *88*, 513-520.
33. Cong, Y. Y.; Chai, C. X.; Zhao, X. W.; Yi, B. L.; Song, Y. J., Pt_{0.25}Ru_{0.75}/N-C as Highly Active and Durable Electrocatalysts toward Alkaline Hydrogen Oxidation Reaction. *Adv. Mater. Interfaces* **2020,** *7* (11), 2000310.
34. Wang, X. N.; Gao, X. C.; Tang, L.; Sun, P. H.; Liu, Y.; Hou, S. Q.; Tong, Y. F.; Yin, X. T.; Ma, X. G., Pt-Sn/Sb Interaction Induces Reversed Charge Transfer and Selective Hydroxyl Adsorption for Enhanced Hydrogen Electro-Oxidation. *Adv. Funct. Mater.* **2024,** *34* (52), 2411206.
35. Liu, D. Q.; Luo, Z. X.; Zhang, B. X.; Zhao, G. Q.; Guo, W.; Chen, J.; Gao, M. X.; Liu, Y. F.; Pan, H. G.; Sun, W. P., Tailoring Interfacial Charge Transfer of Epitaxially Grown Ir Clusters for Boosting Hydrogen Oxidation Reaction. *Adv. Energy Mater.* **2023,** *13* (1), 2202913.
36. Wang, S. P.; Fu, L. H.; Huang, H. P.; Fu, M.; Cai, J. L.; Lyu, Z.; Wang, Q. X.; Kuang, Q.; Xie, Z. X.; Xie, S. F., Local Oxidation Induced Amorphization of 1.5-nm-Thick Pt-Ru Nanowires Enables Superactive and CO-Tolerant Hydrogen Oxidation in Alkaline Media. *Adv. Funct. Mater.* **2023,** *33* (43), 2304125
37. Zhang, J. M.; Qu, X. M.; Shen, L. F.; Li, G.; Zhang, T. N.; Zheng, J. H.; Ji, L. F.; Yan, W.; Han, Y.; Cheng, X. Y.; Jiang, Y. X.; Sun, S. G., Engineering the Near-Surface of PtRu₃ Nanoparticles to Improve Hydrogen Oxidation Activity in Alkaline Electrolyte. *Small* **2021,** *17* (6), 2006698.
38. Wang, H. S.; Abruña, H. D., Designing Synergistic Electrocatalysts for H₂ Oxidation and Evolution Reactions in Alkaline Media. *J. Phys. Chem. C* **2021,** *125* (13), 7188-7203.
39. Qiu, Z. M.; Li, Y.; Gao, Y. D.; Meng, Z. Y.; Sun, Y. Y.; Bai, Y.; Suen, N. T.; Chen, H. C.; Pi, Y. C.; Pang, H., 2D MOF-assisted Pyrolysis-displacement-alloying Synthesis of High-entropy Alloy Nanoparticles Library for Efficient Electrocatalytic Hydrogen Oxidation. *Angew. Chem.-Int. Edit.* **2023,** *62* (33), e202306881.
40. Jiang, J. X.; Liao, J. H.; Tao, S. C.; Najam, T.; Ding, W.; Wang, H. J.; Wei, Z. D., Modulation of iridium-based catalyst by a trace of transition metals for hydrogen oxidation/evolution reaction in alkaline. *Electrochim. Acta* **2020,** *333*, 135444.
41. Dong, Y. T.; Sun, Q. T.; Zhan, C. H.; Zhang, J. T.; Yang, H.; Cheng, T.; Xu, Y.; Hu, Z. W.; Pao, C. W.; Geng, H. B.; Huang, X. Q., Lattice and Surface Engineering of Ruthenium Nanostructures for Enhanced Hydrogen Oxidation Catalysis. *Adv. Funct. Mater.* **2023,** *33* (5), 2210328.
42. Fang, M. M.; Ji, Y. J.; Geng, S. Z.; Su, J. Q.; Li, Y. Y.; Shao, Q.; Lu, J. M., Metastable Metal-Alloy Interface in RuNi Nanoplates Boosts Highly Efficient Hydrogen Electrocatalysis. *ACS Appl. Nano Mater.* **2022,** *5* (12), 17496-17502.

43. Men, Y.; Wu, D.; Hu, Y. C.; Li, L.; Li, P.; Jia, S. F.; Wang, J. B.; Cheng, G. Z.; Chen, S. L.; Luo, W., Understanding Alkaline Hydrogen Oxidation Reaction on PdNiRuIrRh High-Entropy-Alloy by Machine Learning Potential. *Angew. Chem.-Int. Edit.* **2023**, e202217976.
44. Ji, X. F.; Chen, P.; Liu, Y. J.; Ji, Z. Y.; Zhou, H. B.; Chen, C. Y.; Shen, X. P.; Fu, X. Q.; Zhu, G. X., Ir/Ni-NiO/CNT composites as effective electrocatalysts for hydrogen oxidation. *J. Mater. Chem. A* **2023,** *11* (10), 5076-5082.
45. Zhao, L.; Ouyang, B.; Yang, Y. S.; Li, J. T.; Xu, K., Crystal-Phase Engineering of Iridium-Embedded Tungsten for Hydrogen Oxidation Electrocatalysis. *Adv. Funct. Mater.* **2025**, 2420633.
46. Wang, H. S.; Abruña, H. D., IrPdRu/C as H₂ Oxidation Catalysts for Alkaline Fuel Cells. *J. Am. Chem. Soc.* **2017,** *139* (20), 6807-6810.
47. Qin, B. W.; Yu, H. M.; Gao, X. Q.; Yao, D. W.; Sun, X. Y.; Song, W.; Yi, B. L.; Shao, Z. G., Ultrathin IrRu nanowire networks with high performance and durability for the hydrogen oxidation reaction in alkaline anion exchange membrane fuel cells. *J. Mater. Chem. A* **2018,** *6* (41), 20374-20382.
48. Fu, L. H.; Li, Y. B.; Yao, N.; Yang, F. L.; Cheng, G. Z.; Luo, W., IrMo Nanocatalysts for Efficient Alkaline Hydrogen Electrocatalysis. *ACS Catal.* **2020,** *10* (13), 7322-7327.
49. Liu, D.; Lu, S. Q.; Xue, Y. R.; Guan, Z.; Fang, J. J.; Zhu, W.; Zhuang, Z. B., One-pot synthesis of IrNi@Ir core-shell nanoparticles as highly active hydrogen oxidation reaction electrocatalyst in alkaline electrolyte. *Nano Energy* **2019,** *59*, 26-32.
50. Qin, B. W.; Yu, H. M.; Jia, J.; Jun, C.; Gao, X. Q.; Yao, D. W.; Sun, X. Y.; Song, W.; Yi, B. L.; Shao, Z. G., A novel IrNi@PdIr/C core-shell electrocatalyst with enhanced activity and durability for the hydrogen oxidation reaction in alkaline anion exchange membrane fuel cells. *Nanoscale* **2018,** *10* (10), 4872-4881.
51. Wang, X. N.; Tong, Y. F.; Feng, W. T.; Liu, P. Y.; Li, X. J.; Cui, Y. P.; Cai, T. H.; Zhao, L. M.; Xue, Q. Z.; Yan, Z. F.; Yuan, X.; Xing, W., Embedding oxophilic rare-earth single atom in platinum nanoclusters for efficient hydrogen electro-oxidation. *Nat. Commun.* **2023,** *14* (1), 3767.
52. Zhao, P. C.; Deng, L. Q.; Sun, C.; Li, X. P.; Tian, X. Y.; Li, Z.; Sheng, W. C., New Insights into the Roles of Surface and Lattice Hydrogen in Electrocatalytic Hydrogen Oxidation. *ACS Catal.* **2025,** *15* (2), 1352-1362.
53. Ma, M.; Li, G.; Yan, W.; Wu, Z. Z.; Zheng, Z. P.; Zhang, X. B.; Wang, Q. X.; Du, G. F.; Liu, D. Y.; Xie, Z. X.; Kuang, Q.; Zheng, L. S., Single-Atom Molybdenum Engineered Platinum Nanocatalyst for Boosted Alkaline Hydrogen Oxidation. *Adv. Energy Mater.* **2022,** *12* (14), 2103336.
54. Li, L. G.; Liu, S. H.; Zhan, C. H.; Wen, Y.; Sun, Z. F.; Han, J. J.; Chan, T. S.; Zhang, Q. B.; Hu, Z. W.; Huang, X. Q., Surface and lattice engineered ruthenium superstructures towards high-performance bifunctional hydrogen catalysis. *Energy Environ. Sci.* **2023,** *16* (1), 157-166.
55. Zhao, Y. M.; Wu, D.; Luo, W., Correlating Alkaline Hydrogen Electrocatalysis and Hydroxide Binding Energies on Mo-Modified Ru Catalysts. *ACS Sustain.*

Chem. Eng. **2022,** *10* (4), 1616-1623.
56. Tang, T.; Liu, X. Z.; Luo, X.; Xue, Z. Z.; Pan, H. R.; Fu, J. J.; Yao, Z. C.; Jiang, Z.; Lyu, Z. H.; Zheng, L. R.; Su, D.; Zhang, J. N.; Zhang, L.; Hu, J. S., Unconventional Bilateral Compressive Strained Ni-Ir Interface Synergistically Accelerates Alkaline Hydrogen Oxidation. *J. Am. Chem. Soc.* **2023,** *145* (25), 13805-13815.
57. Xiao, W. P.; Lei, W.; Wang, J.; Gao, G. Y.; Zhao, T. H.; Cordeiro, M. A. L.; Lin, R. Q.; Gong, M. X.; Guo, X. Y.; Stavitski, E.; Xin, H. L. L.; Zhu, Y.; Wang, D. L., Tuning the electrocatalytic activity of Pt by structurally ordered PdFe/C for the hydrogen oxidation reaction in alkaline media. *J. Mater. Chem. A* **2018,** *6* (24), 11346-11352.
58. Alia, S. M.; Yan, Y. S., Palladium Coated Copper Nanowires as a Hydrogen Oxidation Electrocatalyst in Base. *J. Electrochem. Soc.* **2015,** *162* (8), F849-F853.
59. Chai, C. X.; Huang, H. L.; Yang, H.; Qin, J. Q.; Sun, C. Y.; Li, Y. P.; Wang, Z. Q.; Zhao, X. W.; Qiu, Z. Y.; Li, T. T.; Li, J. H.; Gao, R.; Zhao, Y.; Cong, Y. Y.; Lv, Y.; Song, Y. J., Highly active and CO-resistant PdRuMo/C with a wide potential-stable window toward alkaline hydrogen oxidation reaction. *Chem. Eng. J.* **2025,** *503*, 158580.
60. Xu, C. L.; Chen, Q.; Ding, R.; Huang, S. T.; Zhang, Y.; Fan, G. Y., Sustainable solid-state synthesis of uniformly distributed PdAg alloy nanoparticles for electrocatalytic hydrogen oxidation and evolution. *Chin. J. Catal.* **2021,** *42* (2), 251-258.
61. Samanta, R.; Mishra, R.; Barman, S., Interface- and Surface-Engineered PdO-RuO₂ Hetero-Nanostructures with High Activity for Hydrogen Evolution/Oxidation Reactions. *ChemSusChem* **2021,** *14* (9), 2112-2125.
62. Su, L. X.; Zhao, Y. M.; Jin, Y. M.; Liu, Z. Y.; Cui, H. S.; Luo, W., Identifying the Role of Hydroxyl Binding Energy in a Non-Monotonous Behavior of Pd-Pd₄S for Hydrogen Oxidation Reaction. *Adv. Funct. Mater.* **2022,** *32* (27), 2113047.
63. Wang, H. S.; Abruña, H. D., Rh and Rh Alloy Nanoparticles as Highly Active H₂ Oxidation Catalysts for Alkaline Fuel Cells. *ACS Catal.* **2019,** *9* (6), 5057-5062.
64. Cai, J. L.; Zhang, X.; Lyu, Z.; Huang, H. P.; Wang, S. P.; Fu, L. H.; Wang, Q. X.; Yu, X. F.; Xie, Z. X.; Xie, S. F., Host-Guest Ensemble Effect on Dual-Pt atom-on-Rh Nanosheets Enables High-Efficiency and Anti-CO Alkaline Hydrogen Oxidation. *ACS Catal.* **2023,** *13* (10), 6974-6982.
65. Wang, M. M.; Wang, M. J.; Zhan, C. H.; Geng, H. B.; Li, Y. H.; Huang, X. Q.; Bu, L. Z., Ultrafine platinum-iridium distorted nanowires as robust catalysts toward bifunctional hydrogen catalysis. *J. Mater. Chem. A* **2022,** *10* (36), 18972-18977.
66. Wei, L. C.; Dong, Y. T.; Yan, W.; Zhang, Y. Q.; Zhan, C. H.; Huang, W. H.; Pao, C. W.; Hu, Z. W.; Lin, H. X.; Xu, Y.; Geng, H. B.; Huang, X. Q., Hollow Pt-Encrusted RuCu Nanocages Optimizing OH Adsorption for Efficient Hydrogen Oxidation Electrocatalysis. *Angew. Chem.-Int. Edit.* **2024**, e202420177.

67. Wu, J.; Zhou, Y. J.; Nie, H. D.; Wei, K. Q.; Huang, H.; Liao, F.; Liu, Y.; Shao, M. W.; Kang, Z. H., Carbon dots regulate the interface electron transfer and catalytic kinetics of Pt-based alloys catalyst for highly efficient hydrogen oxidation. *J. Energy Chem.* **2022,** *66*, 61-67.
68. Wang, K. C.; Yang, H.; Zhang, J. T.; Ren, G. M.; Cheng, T.; Xu, Y.; Huang, X. Q., The exclusive surface and electronic effects of Ni on promoting the activity of Pt towards alkaline hydrogen oxidation. *Nano Res.* **2022,** *15* (7), 5865-5872.
69. Pang, B. B.; Jia, C. Y.; Wang, S. C.; Liu, T.; Ding, T.; Liu, X. K.; Liu, D.; Cao, L. L.; Zhu, M. Z.; Liang, C. H.; Wu, Y.; Liao, Z. L.; Jiang, J.; Yao, T., Self-Optimized Ligand Effect of Single-Atom Modifier in Ternary Pt-Based Alloy for Efficient Hydrogen Oxidation. *Nano Lett.* **2023,** *23* (9), 3826-3834.
70. Jin, Y. C.; Chen, F. Y.; Wang, J. L.; Guo, L. F.; Jin, T.; Liu, H. Z., Lamellar platinum-rhodium aerogels with superior electrocatalytic performance for both hydrogen oxidation and evolution reaction in alkaline environment. *J. Power Sources* **2019,** *435*, 226798.
71. Sun, Y. J.; Zhang, W. S.; Zhang, Q. H.; Li, Y. J.; Gu, L.; Guo, S. J., A general approach to high-entropy metallic nanowire electrocatalysts. *Matter* **2023,** *6* (1), 193-205
72. Cong, Y. Y.; Meng, F. C.; Wang, X. L.; Wang, H. B.; Dou, D.; Li, C. L.; Zhao, Q. P., Uniform PtRu_{0.6} Nanoparticles Supported on Nitrogen-Doped Carbon Obtained from ZIF-8/GO Hybrid with Remarkable Alkaline Hydrogen Oxidation Activity. *J. Electron. Mater.* **2023,** *52* (4), 2388-2395.
73. Zhan, C. H.; Xu, Y.; Bu, L. Z.; Zhu, H. Z.; Feng, Y. G.; Yang, T.; Zhang, Y.; Yang, Z. Q.; Huang, B. L.; Shao, Q.; Huang, X. Q., Subnanometer high-entropy alloy nanowires enable remarkable hydrogen oxidation catalysis. *Nat. Commun.* **2021,** *12* (1), 6261.
74. Wang, Y.; Wang, G. W.; Li, G. W.; Huang, B.; Pan, J.; Liu, Q.; Han, J. J.; Xiao, L.; Lu, J. T.; Zhuang, L., Pt-Ru catalyzed hydrogen oxidation in alkaline media: oxophilic effect or electronic effect? *Energy Environ. Sci.* **2015,** *8* (1), 177-181.
75. Gong, T. Y.; Alghamdi, H.; Raciti, D.; Hall, A. S., Improved Alkaline Hydrogen Oxidation on Strain-Modulated Pt Overlayers at Ordered Intermetallic Pt-Sb Cores. *ACS Energy Lett.* **2023,** *8* (1), 685-690.
76. Yang, F.; Bao, X.; Gong, D.; Su, L.; Cheng, G.; Chen, S.; Luo, W., Rhodium Phosphide: A New Type of Hydrogen Oxidation Reaction Catalyst with Non-Linear Correlated Catalytic Response to pH. *ChemElectroChem* **2019,** *6* (7), 1990-1995.
77. Zhang, Y.; Li, G.; Zhao, Z. L.; Han, L. L.; Feng, Y. G.; Liu, S. H.; Xu, B. Y.; Liao, H. G.; Lu, G.; Xin, H. L.; Huang, X. Q., Atomically Isolated Rh Sites within Highly Branched Rh₂Sb Nanostructures Enhance Bifunctional Hydrogen Electrocatalysis. *Adv. Mater.* **2021,** *33* (43), 9.
78. Zhang, J. T.; Liu, X. Z.; Ji, Y. J.; Liu, X. R.; Su, D.; Zhuang, Z. B.; Chang, Y. C.; Pao, C. W.; Shao, Q.; Hu, Z. W.; Huang, X. Q., Atomic-thick metastable phase RhMo nanosheets for hydrogen oxidation catalysis. *Nat. Commun.* **2023,** *14* (1), 1761.

79. Su, L. X.; Zhao, Y. M.; Jin, Y. M.; Fan, X. R.; Liu, Z. Y.; Luo, W., d-p Orbital hybridization in RhSn catalyst boosts hydrogen oxidation reaction under alkaline electrolyte. *J. Mater. Chem. A* **2022,** *10* (41), 21856-21861.
80. Zhang, J. T.; Ren, G. M.; Li, D. Y.; Kong, Q. Y.; Hu, Z. W.; Xu, Y.; Wang, S. L.; Wang, L.; Cao, M. F.; Huang, X. Q., Interface engineering of snow-like Ru/RuO₂ nanosheets for boosting hydrogen electrocatalysis. *Sci. Bull.* **2022,** *67* (20), 2103-2111.
81. St John, S.; Atkinson, R. W.; Unocic, R. R.; Zawodzinski, T. A.; Papandrew, A. B., Ruthenium-Alloy Electrocatalysts with Tunable Hydrogen Oxidation Kinetics in Alkaline Electrolyte. *J. Phys. Chem. C* **2015,** *119* (24), 13481-13487.
82. Chen, L. G.; Liang, X.; Wang, D. S.; Yang, Z. B.; He, C. T.; Zhao, W.; Pei, J. J.; Xue, Y. R., Platinum-Ruthenium Single Atom Alloy as a Bifunctional Electrocatalyst toward Methanol and Hydrogen Oxidation Reactions. *ACS Appl. Mater. Interfaces* **2022,** *14* (24), 27814-27822.
83. Zhang, J. T.; Fan, X.; Wang, S. L.; Cao, M. F.; Bu, L. Z.; Xu, Y.; Lin, H. P.; Huang, X. Q., Surface Engineered Ru₂Ni Multilayer Nanosheets for Hydrogen Oxidation Catalysis. *CCS Chem.* **2023,** *5* (8), 1931-1941.
84. Zhao, Y. M.; Yang, F. L.; Zhang, W.; Li, Q. H.; Wang, X. W.; Su, L. X.; Hu, X. M.; Wang, Y.; Wang, Z. Z.; Zhuang, L.; Chen, S. L.; Luo, W., High-Performance Ru₂P Anodic Catalyst for Alkaline Polymer Electrolyte Fuel Cells. *CCS Chem.* **2022,** *4* (5), 1732-1744.
85. Su, L. X.; Fan, X. R.; Jin, Y. M.; Cong, H. J.; Luo, W., Hydroxyl-Binding Energy-Induced Kinetic Gap Narrowing between Acidic and Alkaline Hydrogen Oxidation Reaction on Intermetallic Ru₃Sn₇ Catalyst. *Small* **2023,** *19* (11), 2207603.
86. Xue, Y. R.; Shi, L.; Liu, X. R.; Fang, J. J.; Wang, X. D.; Setzler, B. P.; Zhu, W.; Yan, Y. S.; Zhuang, Z. B., A highly-active, stable and low-cost platinum-free anode catalyst based on RuNi for hydroxide exchange membrane fuel cells. *Nat. Commun.* **2020,** *11* (1), 5651.
87. Yang, C. Y.; Li, Y. B.; Ge, C. X.; Jiang, W. Y.; Cheng, G. Z.; Zhuang, L.; Luo, W., The Role of Hydroxide Binding Energy in Alkaline Hydrogen Oxidation Reaction Kinetics on RuCr Nanosheet *Chin. J. Chem.* **2022,** *40* (21), 2495-2501.
88. Li, Y. B.; Yang, C. Y.; Ge, C. X.; Yao, N.; Yin, J. L.; Jiang, W. Y.; Cong, H. J.; Cheng, G. Z.; Luo, W.; Zhuang, L., Electronic Modulation of Ru Nanosheet by d-d Orbital Coupling for Enhanced Hydrogen Oxidation Reaction in Alkaline Electrolytes. *Small* **2022,** *18* (29), 2202404.
89. Zhang, S. Q.; Ren, R. J.; Cao, J.; Zhang, D. Z.; Bai, J. S.; Han, C.; Xiao, L.; Zhuang, L.; Song, P.; Xu, W. L., Ru-MnO Heterostructure Clusters Toward Efficient and CO-Tolerant Alkaline Hydrogen Oxidation Reaction. *Adv. Energy Mater.* **2024**, 2404266.
90. Mao, J. J.; He, C. T.; Pei, J. J.; Liu, Y.; Li, J.; Chen, W. X.; He, D. S.; Wang, D. S.; Li, Y. D., Isolated Ni Atoms Dispersed on Ru Nanosheets: High-Performance Electrocatalysts toward Hydrogen Oxidation Reaction. *Nano Lett.* **2020,** *20* (5), 3442-3448

91. Cong, Y. Y.; Meng, F. C.; Wang, H. B.; Dou, D.; Zhao, Q. P.; Li, C. L.; Zhang, N. S.; Tian, J. Y., RuO2-PdO nanowire networks with rich interfaces and defects supported on carbon toward the efficient alkaline hydrogen oxidation reaction. *J. Energy Chem.* **2023,** *83*, 255-263.
92. Wang, P. C.; Wang, C. L.; Yang, Y.; Chen, S.; Cheng, Z. Y.; Huang, M. X.; Tong, H. G.; Chen, Q. W., RuP Nanoparticles Supported on N, O Codoped Porous Hollow Carbon for Efficient Hydrogen Oxidation Reaction. *Adv. Mater. Interfaces* **2022,** *9* (9), 2102193.
93. Tatus-Portnoy, Z.; Kitayev, A.; Vineesh, T. V.; Tal-Gutelmacher, E.; Page, M.; Zitoun, D., A low-loading Ru-rich anode catalyst for high-power anion exchange membrane fuel cells. *Chem. Commun.* **2020,** *56* (42), 5669-5672
94. Su, L. X.; Jin, Y. M.; Gong, D.; Ge, X.; Zhang, W.; Fan, X. R.; Luo, W., The Role of Discrepant Reactive Intermediates on Ru-Ru₂P Heterostructure for pH-Universal Hydrogen Oxidation Reaction. *Angew. Chem.-Int. Edit.* **2023,** *62* (2), 8.
95. Wu, L. Q.; Su, L. X.; Liang, Q.; Zhang, W.; Men, Y.; Luo, W., Boosting Hydrogen Oxidation Kinetics by Promoting Interfacial Water Adsorption on d-p Hybridized Ru Catalysts. *ACS Catal.* **2023,** *13* (7), 4127-4133.